5456–5467 *Nucleic Acids Research, 2014, Vol. 42, No. 9* *Published online 05 March 2014*
doi: 10.1093/nar/gku173

Genome-wide analysis of regulation of gene expression and H3K9me2 distribution by JIL-1 kinase mediated histone H3S10 phosphorylation in *Drosophila*

Weili Cai[1], Chao Wang[1], Yeran Li[1], Changfu Yao[1], Lu Shen[1], Sanzhen Liu[2], Xiaomin Bao[1], Patrick S. Schnable[2,3], Jack Girton[1], Jørgen Johansen[1] and Kristen M. Johansen[1,*]

[1]Department of Biochemistry, Biophysics, and Molecular Biology, Iowa State University, Ames, IA 50011, USA, [2]Department of Agronomy, Iowa State University, Ames, IA 50011, USA and [3]Data2Bio LLC, Ames, IA 50011, USA

Received November 9, 2012; Revised February 09, 2014; Accepted February 11, 2014

ABSTRACT

In this study we have determined the genome-wide relationship of JIL-1 kinase mediated H3S10 phosphorylation with gene expression and the distribution of the epigenetic H3K9me2 mark. We show in wild-type salivary gland cells that the H3S10ph mark is predominantly enriched at active genes whereas the H3K9me2 mark is largely associated with inactive genes. Comparison of global transcription profiles in salivary glands from wild-type and *JIL-1* null mutant larvae revealed that the expression levels of 1539 genes changed at least 2-fold in the mutant and that a substantial number (49%) of these genes were upregulated whereas 51% were downregulated. Furthermore, the results showed that downregulation of genes in the mutant was correlated with higher levels or acquisition of the H3K9me2 mark whereas upregulation of a gene was correlated with loss of or diminished H3K9 dimethylation. These results are compatible with a model where gene expression levels are modulated by the levels of the H3K9me2 mark independent of the state of the H3S10ph mark, which is not required for either transcription or gene activation to occur. Rather, H3S10 phosphorylation functions to indirectly maintain active transcription by counteracting H3K9 dimethylation and gene silencing.

INTRODUCTION

The JIL-1 kinase localizes specifically to euchromatic interband regions of polytene chromosomes and is the kinase responsible for histone H3S10 phosphorylation at interphase in *Drosophila* (1,2). Genetic interaction assays with *JIL-1* hypomorphic and null allelic combinations demonstrated that JIL-1 can counterbalance the gene-silencing effect of the three major heterochromatin markers H3K9me2, Su(var)3-7 and HP1a on position-effect variegation and that in the absence of histone H3S10 phosphorylation these epigenetic marks spread to ectopic locations on the arms of polytene chromosomes (3–7). These observations suggested a model for a dynamic balance between euchromatin and heterochromatin (3,5,6,8), where the level of gene expression is determined by antagonistic functions of the euchromatic H3S10ph mark on the heterochromatic H3K9me2 mark. In strong support of this model, Wang *et al.* (6,9) recently provided evidence that H3K9me2 levels at reporter genes inversely correlate with their levels of expression and that H3K9me2 levels in turn are regulated by H3S10 phosphorylation. Thus, taken together these findings suggest that a major function of JIL-1-mediated histone H3S10 phosphorylation is to maintain an active state of chromatin by counteracting H3K9 dimethylation and gene silencing (3,6,9,10). In an alternative scenario, Corces *et al.* have proposed that JIL-1 and histone H3S10 phosphorylation are required for active transcription by the RNA polymerase II machinery (11–13). However, the results of these studies have been controversial because it has been demonstrated that RNA polymerase II mediated transcription occurs at robust levels in the absence of H3S10 phosphorylation in *Drosophila* (10,14,15).

In this study, to explore the global interplay between the epigenetic H3S10ph and H3K9me2 chromatin modifications and gene expression, we conducted a genome-wide analysis of their enriched sites and combined it with an analysis of changes to the distribution of the H3K9me2 mark and of whole genome transcription level changes in the absence of H3S10 phosphorylation. In order to have the abil-

*To whom correspondence should be addressed. Tel: +515 294 7959; Fax: 515 294 4858; Email: kristen@iastate.edu
Correspondence may also be addressed to Jørgen Johansen. Tel: +515 294 2358; Email: jorgen@iastate.edu

ity to specifically map and correlate the location of JIL-1 and H3K9me2 with the locations of the histone H3S10 phosphorylation mark, salivary gland cells from third instar larvae were analyzed. Salivary gland nuclei are all at interphase excluding contributions from mitotic histone H3S10 phosphorylation. We found that most of the identified JIL-1 binding peaks located at or near transcription start sites (TSS) whereas peaks for both H3S10ph and H3K9me2 enrichment were located around 600 bp downstream of the TSS. A comparison of the transcriptome profiles of salivary glands from wild-type and *JIL-1* null mutants revealed that the expression levels of 1539 genes changed at least 2-fold in the mutant. Interestingly, out of these genes the expression of 66% of normally active genes was repressed, whereas the expression of most normally inactive genes (77%) was activated. Furthermore, we show that in the absence of H3S10 phosphorylation the H3K9me2 mark redistributes and becomes upregulated on ectopic sites on the chromosome arms, especially on the X-chromosome, and that this H3K9me2 redistribution correlates with the activation of silent genes and the repression of active genes. Taken together, these results provide direct support for the model that H3S10 phosphorylation mainly facilitates gene expression of active genes by maintaining an open chromatin structure at promoter regions by counteracting H3K9 dimethylation.

MATERIALS AND METHODS

Drosophila melanogaster stocks

Fly stocks were maintained according to standard protocols (16). Canton S. was used for wild-type preparations. The $JIL\text{-}1^{z2}$ allele is described in Wang *et al.* (2) and in Zhang *et al.* (17).

ChIP-sequencing and data analysis

For ChIP-sequencing, 50 pairs of salivary glands per sample were dissected from third instar larvae and fixed for 15 min at room temperature in 1 ml of fixative (50-mM HEPES at pH 7.6, 100-mM NaCl, 0.1-mM EDTA at pH 8, 0.5-mM EGTA at pH 8, 2% formaldehyde). Preparation of chromatin for immunoprecipitation was performed as previously described (18). Mouse anti-JIL-1 mAb 5C9 (19), mouse anti-H3K9me2 mAb 1220 (Abcam), or rabbit anti-H3S10ph pAb (Cell Signaling or Active Motif) were used for immunoprecipitation. For each sample, 10% of the chromatin lysate was used as control input DNA, and 90% was immunoprecipitated with the antibody. DNA from the immunoprecipitated chromatin fragments was purified using a Wizard SV DNA purification kit (Promega).

Before sequencing, the purified ChIP-enriched DNA fragments were selected on an agarose gel for fragments 200 bp in size, linkers were added, and the library was amplified by polymerase chain reaction (PCR). Each library was sequenced at the Iowa State University DNA facility by a Genome Analyser II or a Hiseq200 sequencing platform (Illumina). All samples were processed using 36 or 100 bp single-end protocols (Illumina). All reads were mapped to dm3 version 5 of the *Drosophila melanogaster* genome using Bowtie V0.12.7 (20) with the default settings and output to the SAM format. SAMtools V0.1.18 (21) and BEDtools V2.14.3 (22) were used to sort and transfer files. Enriched islands for JIL-1, H3S10ph and H3K9me2 (wild-type and $JIL\text{-}1^{Z2}$/ $JIL\text{-}1^{Z2}$) were identified using SICER V1.1 with 200 bp window size, 200 bp gap size, and an effective genome size of 72% of the *Drosophila* genome (23). Enriched islands with a false discovery rate (FDR) of 1% or less were considered to be valid. MACS V1.4 (24) was used to identify JIL-1 binding peaks with default settings and FDRs of 10% or less. Binding islands or the number of reads obtained in each genomic region scaled to the total number of reads were rendered in the integrated genome viewer (IGV 2.0). ChIP on chip profiles of Chromator were generated from data in Kc cells obtained by ModENCODE (25) and presented as average log2 signal ratio of IP over input. The ChIPpeakAnno bioconductor R package (26) was employed to annotate the binding sites to the nearest start of a gene and to map the distance to the nearest TSS. Density plots of the center of enriched binding islands relative to the distance from the TSS of nearby genes were made using SAS (SAS Institute, Inc).

RNA-sequencing and data analysis

For RNA-sequencing, total RNA from third instar salivary glands was isolated using the UltraClean Tissue and Cells RNA Isolation Kit (Mo Bio). DNA was removed using the DNase I kit (Mo Bio). Two replicated samples of each wild-type and $JIL\text{-}1^{z2}/JIL\text{-}1^{z2}$ null mutant RNA were amplified and sequenced on an Illumina Hiseq2000 at the Iowa State University DNA facility using a paired-end protocol. Low-quality nucleotides were removed from raw reads using Data2Bio's trimming script (27). GSNAP (Genomic Short-read Nucleotide Alignment Program, version 201310–12) (28), which allows for intron-spanning alignments, was used to map trimmed reads to the reference genome (BDGP 5.72/dm3 June 2013). Reads with one unique best match in the reference genome (BDGP 5.72/dm3 June 2013) with $\leq$2 mismatches every 50 bp were used for all subsequent analyses. The read depth of each gene was computed based on the coordinates of mapped reads and the annotated locations of genes in the reference genome (BDGP 5.72/dm3 June 2013). Reads per kilobase of exons per million uniquely mapped reads (RPKM) values were calculated as in Mortazavi *et al.* (29).

For identification of genes with different expression in the *JIL-1* mutant background, the log-scale 75th percentile of library size normalization method was used to normalize wild-type and mutant RNA-Seq reads (30). The normalized reads were counted by HTseq(v0.5.4). The QuasiSeq (R package) was used to identify differentially expressed genes by negative binomial quasi-likelihood estimation (31). Genes were considered differentially expressed between wild-type and the mutant if they exhibited a greater than 2-fold change in expression and an FDR smaller than 0.05. Scatter plot representations of gene expression changes between wild-type and *JIL-1* null mutant salivary gland cells as well as regression analysis were performed using SAS (SAS Institute, Inc). Gene Ontology (GO) term categories for genes identified as down- or upregulated in *JIL-1* null mutant versus wild-type salivary glands were iden-

tified by DAVID (32) in Level 5 of biological process and molecular function. In addition, box plots, bar charts and pie charts were made used using the ggplot2 R package (33) and statistical analysis was performed with R (v3.0.1).

Chromatin immunoprecipitation and qPCR

ChIP experiments were performed as previously described (6,18). In short, for ChIP experiments, 50 pairs of salivary glands per sample were dissected from third instar larvae and fixed for 15 min at room temperature in 1 ml of fixative (50-mM HEPES at pH 7.6, 100-mM NaCl, 0.1-mM EDTA at pH 8, 0.5-mM EGTA at pH 8, 2% formaldehyde). Mouse anti-JIL-1 mAb 5C9 (19), anti-H3K9me2 (Abcam), anti-GST mAb 8C7 (34), anti-H3S10ph (Cell Signaling, Active Motif) or purified rabbit IgG (Sigma) were used for immunoprecipitation. For each sample, the chromatin lysate was divided into equal amounts and immunoprecipitated with experimental and control antibody, respectively. DNA from the immunoprecipitated chromatin fragments (average length, 500 bp) was purified using a Wizard SV DNA purification kit (Promega).

Quantitative PCR was carried out using Brilliant® II SYBR Green QPCR Master Mix (Stratagene) in conjunction with an Mx4000 (Stratagene) PCR machine. The primers used for the various qPCR experiments are listed in Supplementary Table S1. Cycling parameters were 10 min at 95°C, followed by 40 cycles of 30 s at 95°C, 30 s at 55°C and 30 s at 72°C. Fluorescence intensities were plotted against the number of cycles using an algorithm provided by Stratagene. Template levels were quantified using a calibration curve based on dilution of concentrated DNA. For each experimental condition, the relative enrichment was normalized to the corresponding control immunoprecipitation from the same chromatin lysate.

Immunohistochemistry

Polytene chromosome squash preparations were performed as in Cai *et al.* (35) using a 5 min fixation protocol and double labeled with JIL-1 mAb 5C9 (19) and rabbit anti-histone H3K9me2 (Millipore). DNA was counterstained by Hoechst 33258 (Molecular Probes) in phosphate buffered saline. The appropriate species- and isotype-specific TRITC-, and FITC-conjugated secondary antibodies (Cappel/ICN, Southern Biotech) were used (1:200 dilution). The final preparations were mounted in 90% glycerol containing 0.5% *n*-propyl gallate. The preparations were examined using epifluorescence optics on a Zeiss Axioskop microscope and images were captured and digitized using a cooled Spot CCD camera. Images were imported into Photoshop where they were pseudocolored, image processed and merged. In some images non-linear adjustments were made to the channel with Hoechst labeling for optimal visualization of chromosomes.

Modeling of JIL-1

The structure of JIL-1 was modeled with the I-TASSER protein prediction server (36,37) and compared to the crystal structure of a nucleosome (PDB ID: 1AOI). I-TASSER generates models of proteins by excising continuous fragments from Local Meta-Threading-Server multiple-threading alignments and then reassembling them using replica-exchange Monte Carlo simulations (38). The comparison and visualization between the model of JIL-1 and the nucleosome was processed and rendered by PyMOL.

RESULTS

Mapping the genome-wide distribution of JIL-1, H3S10ph and H3K9me2 in salivary gland cells

All DNA and RNA samples analyzed were from post-mitotic third instar larval salivary glands that included both sexes and issues of JIL-1's and H3S10 phosphorylation's role in dosage compensation of the X-chromosome were not addressed in this study. For comparisons of gene transcription and H3K9me2 distribution in the absence of JIL-1 and H3S10 phosphorylation with wild-type we analyzed DNA and RNA from salivary glands of $JIL\text{-}1^{z2}/JIL\text{-}1^{z2}$ homozygous larvae. $JIL\text{-}1^{z2}$ is a true null allele generated by P-element mobilization (2). The global transcription profiles were generated by analysis of two independent RNA-Seq experiments. Based on the formula of Mortazavi *et al.* (29) we calculated that in salivary glands one read per kilobase of exons per million uniquely mapped reads (RPKM) corresponded to approximately one transcript per cell. Thus, genes with an RPKM of one or more were considered active, otherwise they were categorized as inactive. We further classified the active genes into three separate groups with low, moderate or high expression levels reflected by RPKMs of from 1–5, >5–30, or >30, respectively. For ChIP-Seq analysis of JIL-1 genomic binding sites we used a previously characterized and highly specific mAb 5C9 (19) and conducted two independent experiments. Enriched chromatin binding sites were identified using the SICER algorithm (23) (Figure 1A). The resulting two data sets were highly correlated (Supplementary Figure S1) and we identified 2819 genes associated with binding sites enriched for JIL-1 present in both data sets that were used for the following analysis. For ChIP-Seq analysis of the genome-wide distribution of the H3S10ph mark we used two previously validated antibodies (6,9) from Cell Signaling (CS) and Active Motif (AM), respectively. As illustrated in Supplementary Figure S1, the two data sets for these antibodies were strongly correlated and we identified 2948 genes enriched for H3S10ph present in both data sets that were used for the subsequent analysis. For analysis of the H3K9me2 mark we used the mAb 1220 (Abcam) verified for ChIP analysis by ModENCODE (25) as well as by Wang *et al.* (6,9) and determined its global distribution in both wild-type and in the *JIL-1* null mutant background. Based on two independent ChIP-Seq experiments for each condition, we identified 833 genes enriched for H3K9me2 in both data sets for wild-type and 488 genes enriched for H3K9me2 in both data sets from the *JIL-1* null background (Supplementary Figure S1). To further validate our RNA-Seq data we confirmed selected genes with qPCR assays (Supplementary Figure S2).

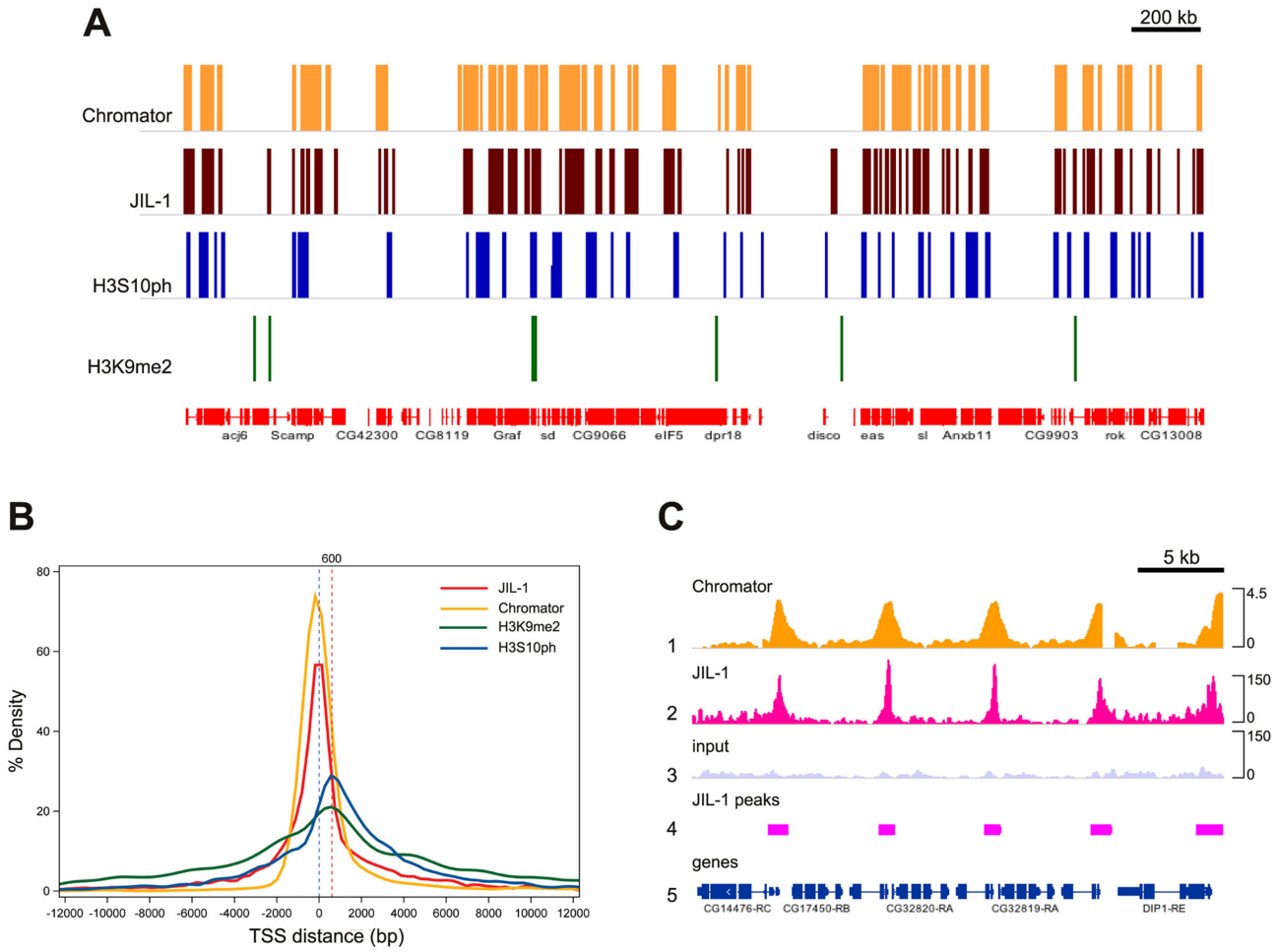

Figure 1. High-resolution profiling of JIL-1, H3S10ph and H3K9me2 enriched genomic regions in *Drosophila* salivary gland cells. (**A**) Comparison of enriched genomic islands for Chromator (data from ModENCODE), JIL-1 (data from JIL-1(data set 2)), H3S10ph (data from H3S10ph(CS antibody)) and H3K9me2 on a section of the X chromosome. The location of genes (in red) is indicated below. The enhanced genomic islands were identified using the SICER algorithm (23) with a 200 bp window and a 200 bp gap size. (**B**) Density of Chromator, JIL-1, H3S10ph and H3K9me2 enriched islands as determined in (A) plotted relative to the distance from the TSS of nearby genes. Chromator and JIL-1 on average tend to localize to enriched islands with a peak centered near the TSS. H3S10ph and H3K9me2 on average tend to localize with a peak about 600 bp after the TSS. (**C**) JIL-1 enriched binding peaks strongly correlate with those of Chromator and are preferentially located at the 5′-end of genes. Lane 1: ChIP on chip profile of Chromator (data from ModENCODE). The data are represented as average log2 signal ratio of immunoprecipitation (IP) over input. Lane 2: ChIP-Seq profile of JIL-1 (data from JIL-1(data set 2)). The height of the peaks represents the number of reads obtained in each region scaled to the total number of reads. Lane 3: ChIP-Seq input profile. The height of the peaks represents the number of reads obtained in each region scaled to the total number of reads. Lane 4: peak JIL-1 enriched binding regions determined by the MACS peak finding algorithm (24). Lane 5: the location of genes in the depicted section of the X chromosome.

Genome-wide DNA-enrichment profiles for JIL-1, H3S10ph and H3K9me2

In order to determine the relative distribution of JIL-1 and the H3S10ph and H3K9me2 marks in salivary gland cells, we generated high-resolution genome-wide DNA-enrichment profiles as exemplified in Figure 1A and Supplementary Figure S3. In addition, we compared these profiles to that of Chromator obtained by ChIP on chip analysis by ModENCODE in Kc cells (25). A caveat to this analysis is that the data are from different cells and tissues. Chromator is a chromodomain-containing protein (34,39) that is a known binding partner of JIL-1 that co-localizes with JIL-1 at interband regions in immunolabeled polytene salivary gland squash preparations (40). To further characterize the enrichment in and around genes, we plotted the distribution of the middle position of the enriched islands (clusters of enriched windows) determined by SICER (23) relative to TSS of genes (Figure 1B). As illustrated in Figure 1B, genome-wide distance correlation revealed that the majority of the identified JIL-1 enriched islands were centered in close proximity to the TSS within ±500 bp and that the peak was aligned near 0 bp. Interestingly, the distribution of Chromator-enriched islands with respect to the TSS was nearly identical to that of JIL-1 (Figure 1B). Furthermore, analysis of discrete binding peaks of JIL-1 determined by the MACS peak-finding algorithm (24) revealed that they were highly correlated with Chromator binding peaks and located preferentially to the 5′-end of genes (Figure 1C). These data suggest that JIL-1 and Chromator share the same specific binding sites although it has been demon-

strated that neither depends on the other for its binding (40). Although the majority of JIL-1 binding peaks map in the proximity of the TSS, we also found the presence of many binding regions at the level of exons, introns and the 3′-end of genes (Figure 1A).

Although H3S10ph enrichment was highly correlated with that of JIL-1 (Figure 1A and Supplementary Figure S1), the profile of H3S10ph was markedly different from that of JIL-1 around the TSS (Figure 1B). H3S10ph's distribution was much broader and the peak enrichment was shifted to about 600 bp downstream of the TSS. Furthermore, only 35% of JIL-1-enriched genes were concomitantly enriched for the H3S10ph mark. This suggests that JIL-1 may not phosphorylate histone H3 at the nucleosome to which it is bound. To explore this possibility, we modeled the 3D structure of JIL-1 using the I-TASSER structure prediction program (37) and compared it to the nucleosome crystal structure (41). As illustrated in Supplementary Figure S4, considering that JIL-1 is known to bind the tail of H3 by the end of its carboxy-terminal domain (42) and that its folded structure is larger than a nucleosome, it is likely to have the capacity to phosphorylate histone H3 of one or more nucleosomes some distance away from its actual binding site depending on the state of higher order nucleosome packaging. Thus, as indicated by the present data, the distribution of JIL-1 and H3S10 phosphorylation may not necessarily be coincident. Interestingly, the distribution of H3K9me2 binding around the TSS closely mirrored that of H3S10ph (Figure 1B), indicating that these two epigenetic modifications may occur in similar genomic contexts.

H3S10 phosphorylation is enriched at active genes and correlated with enhanced gene expression

JIL-1-mediated H3S10 phosphorylation has been proposed to maintain an active state of chromatin (43). Consistent with this hypothesis we found that enrichment of JIL-1 and the H3S10ph mark predominantly were associated with active genes (79% and 67%, respectively) (Figure 2A). In contrast, enrichment of the H3K9me2 mark had a more pronounced association with inactive genes (47%) (Figure 2A). However, it should be noted that JIL-1 and the H3S10ph mark were also enriched at many inactive genes (21% and 33%, respectively) whereas the enrichment of the H3K9me2 mark in many cases was associated with active genes (53%) (Figure 2A). Thus, to further explore the correlation of gene expression's dependence on the presence of the H3S10ph and H3K9me2 marks we determined the average gene expression of genes enriched for the H3S10ph or H3K9me2 mark only and genes enriched for both marks. As illustrated in Figure 2B, the median gene expression for these groups of genes was significantly different from each other with the highest expression of genes enriched for the H3S10ph mark only and lowest expression of genes enriched with the H3K9me2 mark only, whereas gene expression for genes enriched for both marks was intermediate. We further compared the relative proportions of high expression, moderate expression, low expression and inactive genes associated with enriched levels of the H3S10ph or H3K9me2 mark only and genes enriched for both marks (Figure 2C). The results show that the proportion of high, moderate and low expression genes was greater when associated with enriched levels of the H3S10ph mark only and conversely that the proportion of inactive genes increased with enriched levels of the H3K9me2 mark only. The relative proportion of high, moderate and low expressing genes was intermediate between genes with enrichment for both marks compared to the distribution of these classes of genes with single marks (Figure 2C). Thus, taken together these results suggest that at a genome-wide level the enrichment for the H3S10ph mark is directly correlated with enhanced gene expression.

Loss of JIL-1 and H3S10 phosphorylation lead to both gene up- and downregulation

In order to determine the changes in gene transcription in the absence of H3S10 phosphorylation, we compared global transcription profiles in salivary glands in two biological replicates from wild-type and $JIL\text{-}1^{z2}/JIL\text{-}1^{z2}$ homozygous null larvae, respectively. The replicate determinations were highly correlated with Pearson's coefficients (R^2) of 0.977 for the two wild-type samples and 0.998 for the two samples from *JIL-1* null larvae. The results showed that out of nearly 15,000 genes analyzed, the expression levels of 1539 genes changed at least 2-fold and with an FDR smaller than 0.05. Interestingly, 51% of these genes were downregulated whereas 49% showed increased expression levels in the *JIL-1* null mutant background. This is illustrated in the scatterplot in Figure 3A where each dot represents the changes in the expression level of each individual gene and in the box plot in Figure 3B. We further plotted the changes in gene expression levels of genes that were classified as active or inactive in wild-type salivary glands. As shown in the box plot in Figure 3C, there was a significant difference in the expression changes between the two groups of genes. Most inactive genes had increased expression in the mutant background whereas active genes on average had a modest decrease. However, when active genes were further divided into groups with low, moderate and high expression, there was a clear trend that the higher the wild-type expression levels of a gene the more its expression levels were decreased in the mutant background (Figure 3D). These data suggest in general that active genes become repressed but that many hitherto inactive genes become activated in the absence of H3S10 phosphorylation.

We next analyzed the up- and downregulated genes in terms of their GO categories (Figure 3E). Strikingly, the results indicate that the downregulated set of genes in the mutant is enriched in categories related to salivary gland function and development whereas the upregulated list is enriched in DNA repair, cellular response to stress, and RNA processing and metabolism categories. That genes in salivary gland and tissue development specific pathways were particularly affected by downregulation in the mutant suggests that H3S10 phosphorylation may play a key role in keeping tissue and developmentally stage-specific genes transcriptionally active.

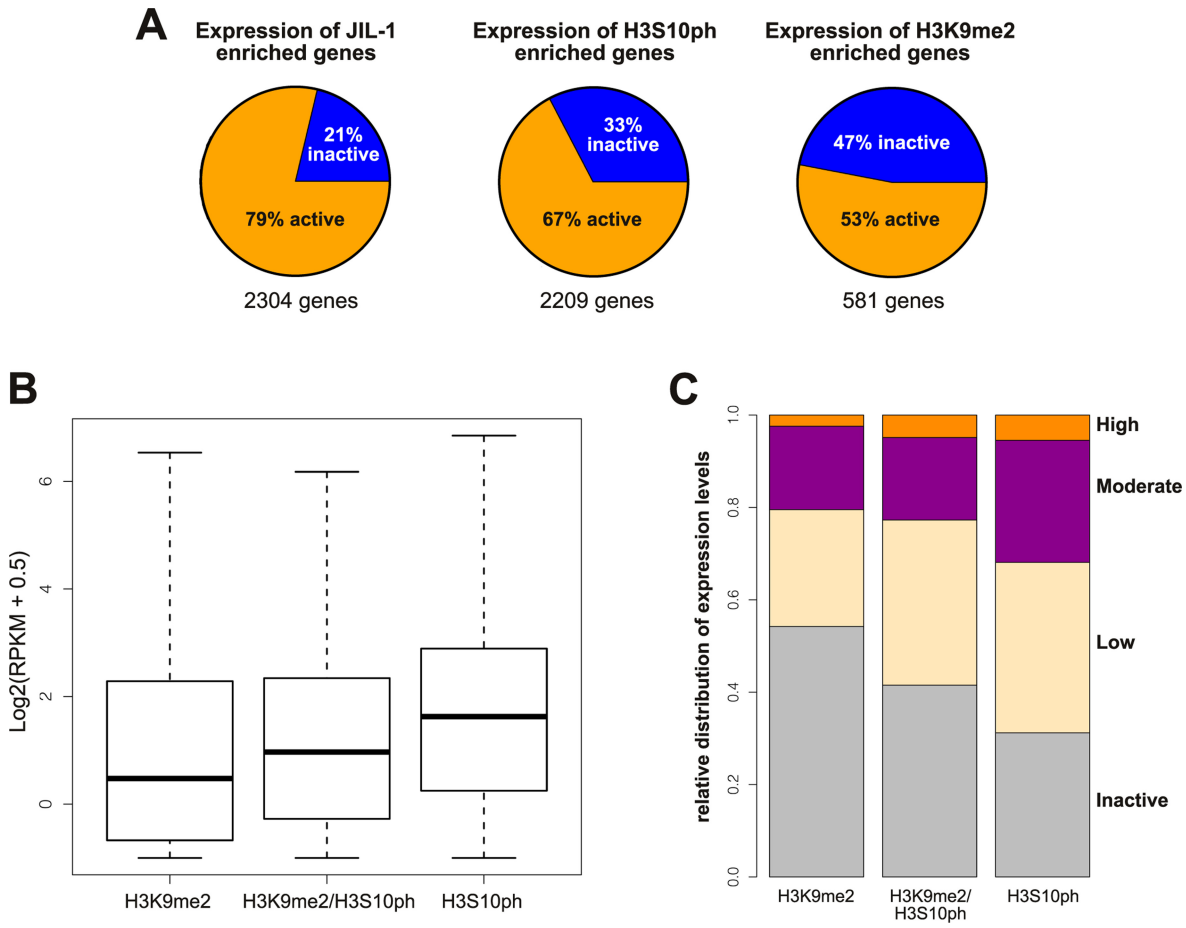

Figure 2. Expression levels of genes enriched for JIL-1, H3S10ph and/or H3K9me2. (**A**) Pie charts of the relative proportion of inactive and active (RPKM≥1) genes enriched for JIL-1, H3S10ph, or H3K9me2, respectively. (**B**) Comparison of the expression of genes enriched for the H3K9me2 or H3S10ph mark only and genes enriched for both marks. Gene expression is represented as log2(RPKM + 0.5). The box plot representation in this and subsequent figures defines 25th to 75th percentiles (boxes), 50th percentile (lines in boxes) and ranges (whiskers, 1.5 times the interquartile range extended from both ends of the box or the maximal/minimal value). Outliers were removed from the analysis. The distribution of gene expression for all three categories was significantly different from each other (P-values < 0.005; Pairwise Wilcoxon Rank Sum Tests). (**C**) Stack bar charts showing the distribution of expression of genes enriched for the H3K9me2 or H3S10ph mark only and genes enriched for both marks. Genes with an RPKM of less than one were categorized as inactive whereas active genes were separated into three groups with low, moderate, or high expression levels reflected by RPKMs of from 1–5, >5–30, or >30.

H3K9me2 redistribution in the absence of H3S10 phosphorylation correlates with activation of silent genes and repression of active genes

One of the consequences of the absence of H3S10 phosphorylation is a redistribution of the H3K9me2 mark from pericentric heterochromatin to the euchromatic regions of the chromosome arms (3–7). This is illustrated by the H3K9me2 immunolabeling of polytene squash preparations from wild-type and *JIL-1* null mutant salivary glands in Figure 4A with the redistribution especially prominent on the X-chromosome of both males and females (3). Thus, to further investigate this redistribution on a genome-wide level we generated maps of H3K9me2 binding by plotting normalized read numbers in 200 bp bins across the genome from wild-type and *JIL-1* null salivary glands. Figure 4B shows an example of such maps comparing wild-type and *JIL-1* mutant X-chromosomes. The results show that in the *JIL-1* null mutant background the levels of H3K9me2 on the chromosome arms were markedly increased and that enriched levels occurred at sites previously not occupied by significant levels of the H3K9me2 mark. Interestingly, although the H3K9me2 mark was enriched on the X-chromosome compared to the autosomes, overall gene expression levels were not statistically different (Figure 4C).

The study of Wang *et al.* (9) of gene expression of the *white* locus provided evidence that H3K9me2 levels at the *white* gene directly correlated with its level of expression and that the H3K9me2 levels in turn were regulated by H3S10 phosphorylation. Based on these findings we reasoned that in the absence of H3S10 phosphorylation gene repression should correlate with increased H3K9me2 binding to the gene, whereas gene activation should be correlated with a loss or decreased H3K9me2 binding. To explore this hypothesis, we plotted the expression of all moderate and high expression genes in our data set without enriched levels of H3K9me2 that acquired the H3K9me2 mark in the *JIL-1* mutant. As illustrated by the box plots in Figure 5A, for 94 such genes there was a significant decrease in their aver-

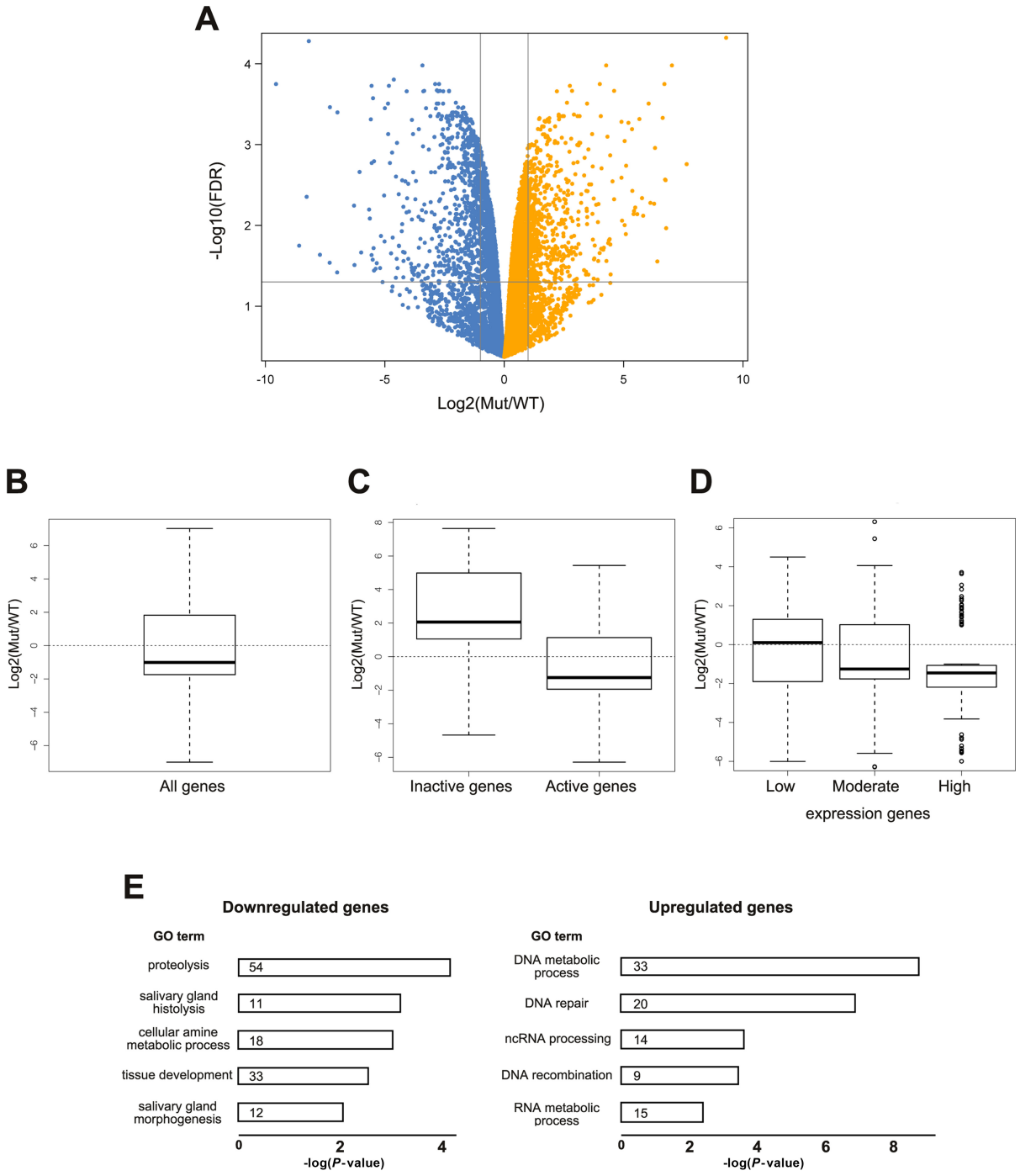

Figure 3. Gene expression can be either down- or upregulated in the absence of H3S10 phosphorylation. (**A**) Scatter plot of gene expression changes between wild-type and *JIL-1* null mutant salivary gland cells. Negative $\log_{10}$(*P*-values) from Fisher's exact test were plotted against the $\log_2$(mutant/wild-type) fold change for each gene. Each dot represents a separate gene. Gray lines indicate the cutoffs for 2-fold changes with a FDR equal to 0.05. Downregulated genes in the *JIL-1* mutant are highlighted in light blue and upregulated genes in orange. (**B**) Box plot of gene expression changes between wild-type and *JIL-1* null mutant salivary gland cells of all genes changed at least 2-fold represented as log2(mutant/wild-type) fold change for each gene. The overall changes in gene expression between the mutant and wild-type were not statistically significant (*P*-value = 0.3; Wilcoxon Signed Rank Test). (**C**) Box plot of gene expression changes between wild-type and *JIL-1* null mutant salivary gland cells of inactive versus active (RPKM ≥ 1) genes that changed at least 2-fold represented as log2(mutant/wild-type) fold change for each gene. The distribution of gene expression for the two categories was significantly different from each other (*P*-value < 0.0001; Wilcoxon Rank Sum Test). (**D**) Box plot of gene expression changes between wild-type and *JIL-1* null mutant salivary gland cells of active genes separated into three groups with low, moderate, or high expression levels (RPKMs of from 1–5, >5–30, or >30, respectively) that changed at least 2-fold represented as log2(mutant/wild-type) fold change for each gene. The distribution of gene expression for all three categories was significantly different from each other (low to moderate: *P*-value < 0.01; moderate to high: *P*-value < 0.05; low to high: *P*-value < 0.0001; Pairwise Wilcoxon Rank Sum Tests). (**E**) Gene Ontology (GO) term of JIL-1 enriched genes identified as downregulated (left) or upregulated (right) in *JIL-1* null mutant versus wild-type salivary glands from third instar larvae. The number of genes in each category is shown within the bars. The GO term enrichment was identified by DAVID (32) in Level 5 of biological process and molecular function.

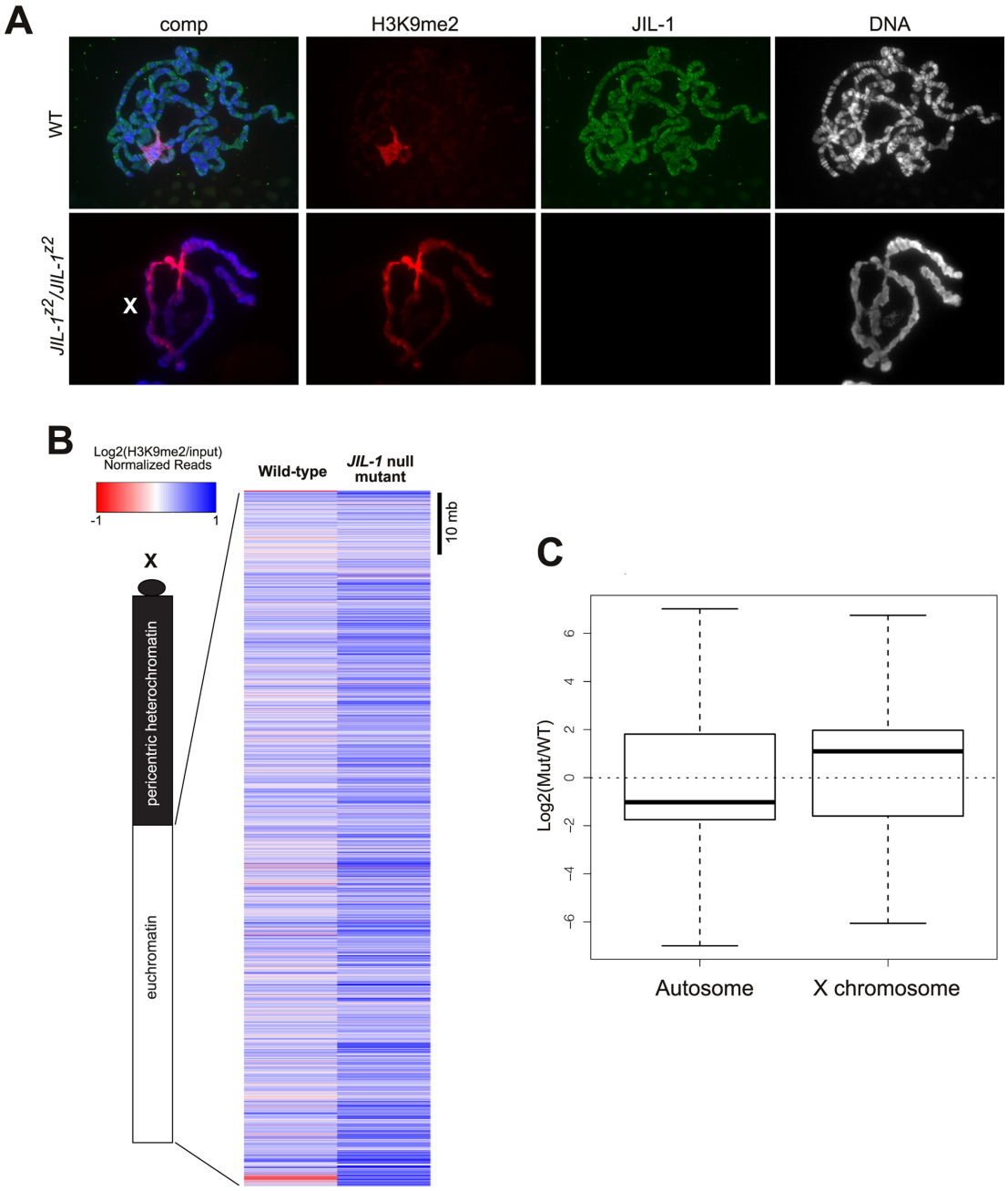

Figure 4. H3K9me2 is redistributed and upregulated on the X-chomosome in *JIL-1* null mutants. (**A**) Wild-type (WT) and *JIL-1* mutant ($JIL\text{-}1^{z2}/JIL\text{-}1^{z2}$) polytene squash preparations labeled with antibody to JIL-1 (in green), H3K9me2 (in red) and with Hoechst (DNA, in blue/gray). The X-chromosome in the *JIL-1* mutant is indicated with an 'X.' (**B**) Comparison of H3K9me2 distribution in wild-type and *JIL-1* null mutants. The maps show normalized (linear normalization by total library size) read numbers (log2(H3K9me2/input)) in 200 bp bins across the X-chromosome scaled from −1 (dark red) to +1 (dark blue). (**C**) Box plot of gene expression changes between wild-type and *JIL-1* null mutant salivary gland cells of autosomal versus X-chromosomal genes that changed at least 2-fold represented as log2(mutant/wild-type) fold change for each gene. The distribution of gene expression for the two categories was similar (P-value = 0.4; Wilcoxon Rank Sum Test).

age levels of expression. To further validate these findings, we performed ChIP assays as in Wang *et al.* (6,9) for five randomly selected genes among the genes analyzed above. Chromatin was immunoprecipitated (ip) from wild-type or *JIL-1* null mutant larval salivary glands using rabbit anti-H3S10ph antibody or purified rabbit IgG antibody (negative control) or mAbs to H3K9me2 or GST (negative control). Primers specific for each of the selected genes were used to amplify the precipitated material. Experiments were done in triplicate and relative enrichment of DNA from the H3S10ph and H3K9me2 ips were normalized to the corresponding control antibody ips performed in tandem for each experimental sample. As illustrated in Figure 5B, at all five genes the relative enrichment of H3S10ph in the mutant was reduced to background levels whereas there was a significant increase of from 2- to 7-fold of the enrichment

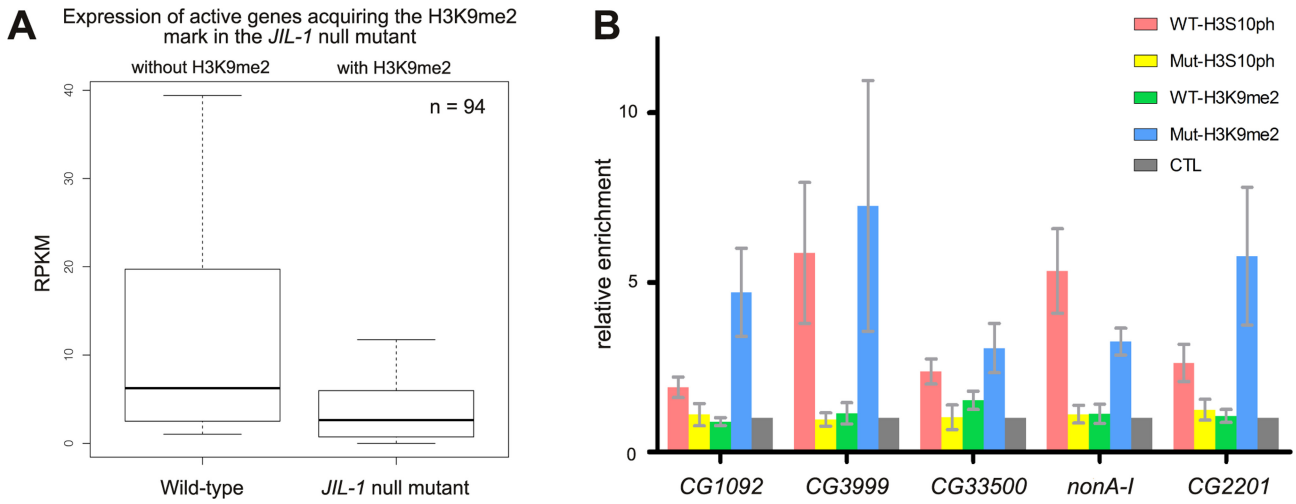

Figure 5. Downregulation of moderate and high expression genes acquiring the H3K9me2 mark in the *JIL-1* null mutant. (**A**) Box plots of RPKM of active genes (RPKM $\geq$ 1) in wild-type that acquire the H3K9me2 mark in the *JIL-1* null mutant background. The distribution of gene expression between the two categories was significantly different (P-value < 0.0001; Wilcoxon Rank Sum Test). (**B**) ChIP analysis of randomly selected active genes in wild-type that are downregulated in the *JIL-1* null mutant background. Histograms show the relative enrichment of chromatin immunoprecipitated by anti-H3K9me2 or anti-H3S10ph antibodies from third instar larval salivary glands from wild-type (WT) and *JIL-1* null mutant larvae. For each experimental condition the average relative enrichment normalized to the corresponding control immunoprecipitation with anti-GST or anti-IgG antibody from three independent experiments with standard deviation is shown. The difference in H3K9me2 levels for all five genes between wild-type and *JIL-1* null salivary glands was statistically significant (P-values < 0.05; two-tailed Student's t-tests).

of the H3K9me2 mark. We next plotted the expression of all inactive and low expression genes in our data set that lost the H3K9me2 mark in the *JIL-1* mutant. The box plots in Figure 6A show that for 69 such genes there was a significant increase in their average levels of expression. As above we validated these findings by performing ChIP assays for five randomly selected genes among the genes analyzed. The results show that at all five genes there was a significant decrease of from 2- to 6-fold of the enrichment of the H3K9me2 mark (Figure 6B). Furthermore, the results confirm that in this class of inactive genes there were very low wild-type levels of H3S10ph. Taken together, these findings suggest that H3S10 phosphorylation modulates H3K9 dimethylation and that H3K9me2 redistribution in the absence of H3S10 phosphorylation correlates with activation of silent genes that lose the H3K9me2 mark and repression of active genes that acquire the H3K9me2 mark.

DISCUSSION

In this study we have determined the relationship of JIL-1 kinase mediated H3S10 phosphorylation with gene expression and the distribution of the epigenetic H3K9me2 mark. We show in wild-type salivary gland cells that the H3S10ph mark is predominantly enriched at active genes whereas the H3K9me2 mark is largely associated with inactive genes. Furthermore, our data demonstrate that discrete binding peaks of JIL-1 are located preferentially to the 5′-end of genes near the TSS and that these peaks are coincident with binding peaks for the chromodomain protein, Chromator, a known binding partner for JIL-1 (40). This distribution of JIL-1 around the TSS is similar to that obtained by ChIP-Seq by Kellner *et al.* (13) in Kc cells but differs from that reported by Regnard *et al.* (10) using ChIP-chip analysis on custom tiling arrays in S2 cells. These latter workers found JIL-1 to be more or less equally distributed along the entire length of genes; however, this result may be a consequence of using lower affinity polyclonal antibodies combined with the lower resolution ChIP-chip approach. Interestingly, we found that although the enrichment profile of H3S10ph was highly correlated with that of JIL-1, the two profiles were not identical. The distribution of the H3S10ph mark was much broader and peak enriched regions were shifted about 600 bp downstream of the TSS. Modeling of the 3D structure of JIL-1 relative to nucleosome structure suggested that a reason for this lack of overlap is that JIL-1 may have the capacity to phosphorylate the tail of H3 of one or more nucleosomes some distance away from its actual binding site depending on the state of higher order nucleosome packaging.

Comparison of global transcription profiles in salivary glands from wild-type and *JIL-1* null mutant larvae revealed that of the nearly 15 000 genes analyzed the expression levels of 1539 genes changed at least 2-fold in the mutant. Surprisingly, among these genes almost as many (49%) increased their expression as were downregulated (51%). This raised the question whether certain classes of genes were preferentially up- or downregulated and further analysis suggested that in general active genes became repressed, whereas hitherto inactive genes became activated in the absence of H3S10 phosphorylation. Furthermore, the results showed that downregulation of genes in the mutant was correlated with higher levels or acquisition of the H3K9me2 mark whereas upregulation of a gene was correlated with loss of or diminished H3K9 dimethylation. These findings directly demonstrate that H3S10 phosphorylation is not required for transcription or gene activation in *Drosophila* as proposed by Corces *et al.* (11–13). This conclusion is further supported by recent experiments by Wang *et al.* (9) analyz-

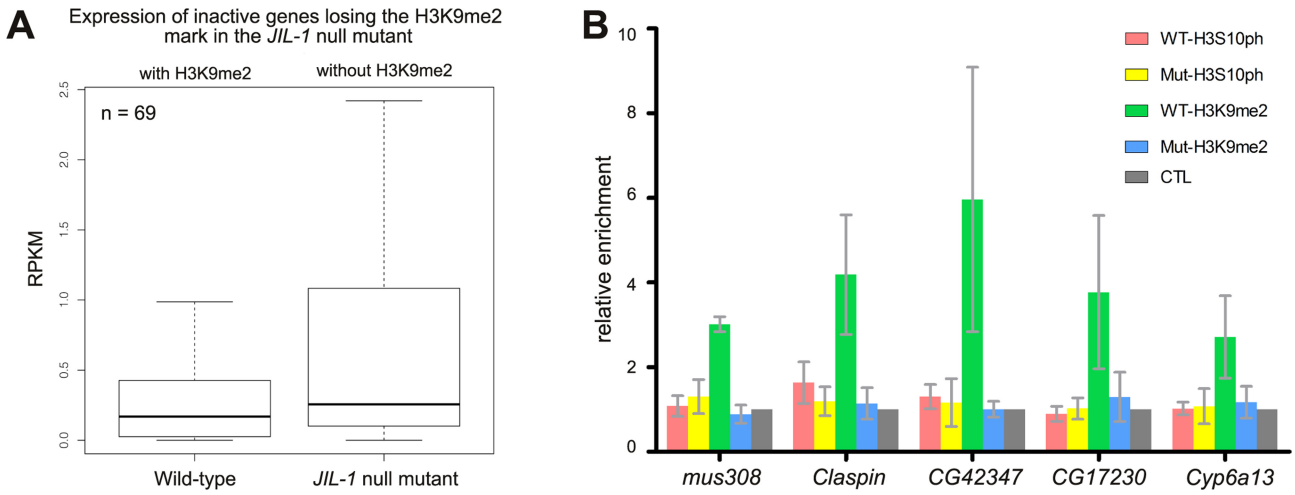

Figure 6. Upregulation of inactive genes losing the H3K9me2 mark in the *JIL-1* null mutant. (**A**) Box plots of RPKM of inactive genes (RPKM < 1) in wild-type that lose the H3K9me2 mark in the *JIL-1* null mutant background. The distribution of gene expression between the two categories was significantly different (*P*-value < 0.005; Wilcoxon Rank Sum Test). (**B**) ChIP analysis of randomly selected inactive genes in wild-type that are upregulated in the *JIL-1* null mutant background. Histograms show the relative enrichment of chromatin immunoprecipitated by anti-H3K9me2 or anti-H3S10ph antibodies from third instar larval salivary glands from wild-type (WT) and *JIL-1* null mutant larvae. For each experimental condition the average relative enrichment normalized to the corresponding control immunoprecipitation with anti-GST or anti-IgG antibody from three independent experiments with SD is shown. The difference in H3K9me2 levels for all five genes between wild-type and *JIL-1* null salivary glands was statistically significant (*P*-values < 0.05; two-tailed Student's t-tests).

ing *white* gene expression where levels of the H3S10ph mark can be manipulated and correlated with the resulting levels of the H3K9me2 mark using ChIP assays. In wild-type, there are moderate levels of the H3S10ph mark and low levels of the epigenetic H3K9me2 mark at the *white* gene resulting in its normal expression. However, in the w^{m4} allele heterochromatic factors can spread across the inversion breakpoint (5,6,43,44) leading to high levels of H3K9me2 at the *white* gene and silencing of gene expression. Interestingly, Wang *et al.* (9) demonstrated that this increase in H3K9me2 level can be prevented by ectopic H3S10 phosphorylation at the *white* gene restoring gene expression. In contrast, in the absence of H3S10 phosphorylation as it occurs in strong *JIL-1* hypomorphic mutant backgrounds, there is a redistribution of heterochromatic factors to ectopic chromosome sites resulting in reduced levels of these factors at the pericentric heterochromatin (3). This leads to less heterochromatic spreading and lower levels of H3K9me2 at the *white* gene in the w^{m4} inversion, thus allowing for increased *white* gene expression (9). Thus, taken together these results are compatible with a model (Figure 7) where gene expression levels are directly correlated with the levels of the H3K9me2 mark independent of the state of the H3S10ph mark, which is not required for either transcription or gene activation to occur. However, H3S10 phosphorylation functions to indirectly regulate transcription by counteracting H3K9 dimethylation and gene silencing in a finely tuned balance (3,5,6,8).

That genes in GO categories for salivary gland specific pathways were particularly affected by downregulation in a *JIL-1* mutant background suggests that H3S10 phosphorylation may serve to keep genes transcriptionally active in a tissue and/or developmentally stage-specific context. How JIL-1 and H3S10 phosphorylation get targeted to specific sets of genes is not known. However, it has been suggested as a general model that JIL-1 targeting to active chromatin may be facilitated by or dependent on the presence of the H3K36me2 and H4K16ac marks (10). Interestingly, the GO categories for genes becoming activated or upregulated in the absence of H3S10 phosphorylation were enriched in DNA repair, DNA and RNA metabolism, and cellular response to stress pathways. Upregulation of such genes would be consistent with a cellular attempt to compensate for the general downregulation of active genes and to the gross perturbation of chromatin structure occurring in *JIL-1* null mutant backgrounds (2,45). If this represents a

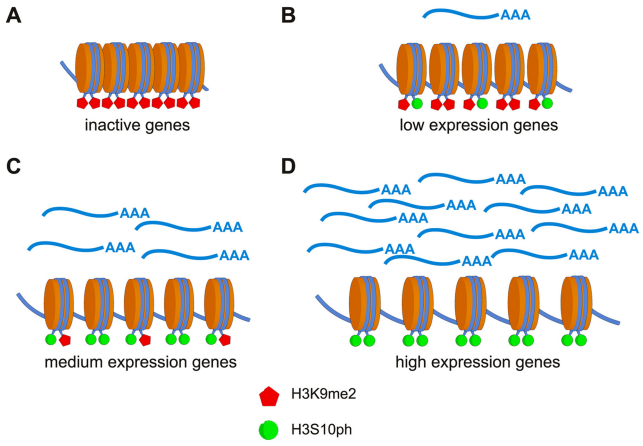

Figure 7. Model for indirect regulation of gene expression by H3S10 phosphorylation. (**A**) At inactive genes, high levels of H3K9 dimethylation lead to a compact chromatin configuration and gene silencing. (**B–D**) At active genes, H3S10 phosphorylation counteracts H3K9 dimethylation leading to a more open chromatin structure facilitating gene expression. In this model, gene expression levels are directly correlated with the levels of the H3K9me2 mark independent of the state of the H3S10ph mark, which is not required for either transcription or gene activation to occur.

specific response to alterations in the mutant, it implies activation of unknown gene induction pathways independent of H3S10 phosphorylation. However, an alternative scenario is that when the H3S10ph mark, which normally serves to limit heterochromatic spreading, is lost in the *JIL-1* mutant, the H3K9me2 silencing mark can now disperse away from previously repressed locations, resulting in transcriptional activation of the now unmasked genes.

In summary, the findings of this study indicate that a major functional role of JIL-1-mediated H3S10 phosphorylation is to maintain active gene expression by serving as a protective epigenetic mark counteracting H3K9 dimethylation and gene silencing. This suggests that different gene expression profiles are regulated by strategic deployment of silencing marks within the genome, and that H3S10 phosphorylation can be an effective means of counteracting silencing effects. This may also be relevant in other organisms where H3S10ph is implicated in the rapid yet transient induction of promoters in response to various inducers (46,47).

ACCESSION NUMBERS

The ChIP-Seq and RNA-Seq data have been deposited in the NCBI Gene Expression Omnibus (http://www.ncbi.nlm.nih.gov/geo) under accession number GSE41047.

SUPPLEMENTARY DATA

Supplementary Data are available at NAR Online, including Supplementary Figures S1–S4 and Supplementary Table S1.

ACKNOWLEDGMENTS

We thank Dr D. Nettleton and members of the laboratory for discussion and advice. We also wish to acknowledge Mr Atrez Norwood and Mr Cheng-Ting Yeh for technical assistance.

FUNDING

National Institutes of Health [GM062916 to K.M.J. and J.J.].

REFERENCES

1. Jin,Y., Wang,Y., Walker,D.L., Dong,H., Conley,C., Johansen,J. and Johansen,K.M. (1999) JIL-1: a novel chromosomal kinase implicated in transcriptional regulation in *Drosophila*. *Mol. Cell*, **4**, 129–135.
2. Wang,Y., Zhang,W., Jin,Y., Johansen,J. and Johansen,K.M. (2001) The JIL-1 tandem kinase mediates histone H3 phosphorylation and is required for maintenance of chromatin structure in *Drosophila*. *Cell*, **105**, 433–443.
3. Zhang,W., Deng,H., Bao,X., Lerach,S., Girton,J., Johansen,J. and Johansen,K.M. (2006) The JIL-1 histone H3S10 kinase regulates dimethyl H3K9 modifications and heterochromatic spreading in *Drosophila*. *Development*, **133**, 229–235.
4. Deng,H., Bao,X., Zhang,W., Girton,J., Johansen,J. and Johansen,K.M. (2007) Reduced levels of Su(var)3-9 but not Su(var)2-5 (HP1) counteract the effects on chromatin structure and viability in loss-of-function mutants of the JIL-1 histone H3S10 kinase. *Genetics*, **177**, 79–87.
5. Deng,H., Cai,W., Wang,C., Lerach,S., Delattre,M., Girton,J., Johansen,J. and Johansen,K.M. (2010) *JIL-1* and *Su(var)3-7* interact genetically and counterbalance each others' effect on position effect variegation in *Drosophila*. *Genetics*, **185**, 1183–1192.
6. Wang,C., Cai,W., Li,Y., Deng,H., Bao,X., Girton,J., Johansen,J. and Johansen,K.M. (2011) The epigenetic H3S10 phosphorylation mark is required for counteracting heterochromatic spreading and gene silencing in *Drosophila melanogaster*. *J. Cell Sci.*, **124**, 4309–4317.
7. Wang,C., Girton,J., Johansen,J. and Johansen,K.M. (2011) A balance between euchromatic (JIL-1) and heterochromatic (SU(VAR)2-5 and SU(VAR)3-9) factors regulates position-effect variegation in *Drosophila*. *Genetics*, **188**, 745–748.
8. Ebert,A., Schotta,G., Lein,S., Kubicek,S., Krauss,V., Jenuwein,T. and Reuter,G. (2004) *Su(var)* genes regulate the balance between euchromatin and heterochromatin in *Drosophila*. *Genes Dev.*, **18**, 2973–2983.
9. Wang,C., Cai,W., Li,Y., Girton,J., Johansen,J. and Johansen,K.M. (2012) H3S10 phosphorylation by the JIL-1 kinase regulates H3K9 dimethylation and gene expression at the *white* locus in *Drosophila*. *Fly*, **6**, 1–5.
10. Regnard,C., Straub,T., Mitterweger,A., Dahlsveen,I.K., Fabian,V. and Becker,P.B. (2011) Global analysis of the relationship between JIL-1 kinase and transcription. *PLoS Genetics*, **7**, e1001327.
11. Ivaldi,M.S., Karam,C.S. and Corces,V.G. (2007) Phosphorylation of histone H3 at Ser10 facilitates RNA polymerase II release from promoter-proximal pausing in *Drosophila*. *Genes Dev.*, **21**, 2818–2831.
12. Karam,C.S., Kellner,W.A., Takenada,N., Clemmons,A.W. and Corces,V.G. (2010) 14-3-3 mediates histone cross-talk during transcription elongation in *Drosophila*. *PLoS Genetics*, **6**, e1000975.
13. Kellner,W.A., Ramos,E., Bortle,K.V., Takenada,N. and Corces,V.G. (2012) Genome-wide phosphoacetylation of histone H3 at *Drosophila* enhancers and promoters. *Genome Res.*, **22**, 1081–1088.
14. Wang,C., Yao,C., Li,Y., Cai,W., Girton,J., Johansen,J. and Johansen,K.M. (2012) Evidence against a role for the JIL-1 kinase in H3S28 phosphorylation and 14-3-3 recruitment to active genes in *Drosophila*. *PLoS ONE*, **8**, e62484.
15. Cai,W., Bao,X., Deng,H., Jin,Y., Girton,J., Johansen,J. and Johansen,K.M. (2008) RNA polymerase II-mediated transcription at active loci does not require histone H3S10 phosphorylation in *Drosophila*. *Development*, **135**, 2917–2925.
16. Roberts,D.B. (1998) Drosophila*: A Practical Approach*, 2nd edn. IRL Press, Oxford, UK.
17. Zhang,W., Jin,Y., Ji,Y., Girton,J., Johansen,J. and Johansen,K.M. (2003) Genetic and phenotypic analysis of alleles of the *Drosophila* chromosomal JIL-1 kinase reveals a functional requirement at multiple developmental stages. *Genetics*, **165**, 1341–1354.
18. Legube,G., McWeeney,S.K., Lercher,M.J. and Akhtar,A. (2006) X-chromosome-wide profiling of MSL-1 distribution and dosage compensation in *Drosophila*. *Genes Dev.*, **20**, 871–883.
19. Jin,Y., Wang,Y., Johansen,J. and Johansen,K.M. (2000) JIL-1, a chromosomal kinase implicated in regulation of chromatin structure, associates with the MSL dosage compensation complex. *J. Cell Biol.*, **149**, 1005–1010.
20. Langmead,B., Trapnell,C., Pop,M. and Salzberg,S.L. (2009) Ultrafast and memory-efficient alignment of short DNA sequences to the human genome. *Genome Biol.*, **10**, R25.
21. Li,H., Handsaker,B., Wysoker,A., Fennell,T., Ruan,J., Homer,N., Marth,G., Abecasis,G. and Durbin,R. (2009) The Sequence Alignment/Map format and SAMtools. *Bioinformatics*, **25**, 2078–2079.
22. Quinlan,A.R. and Hall,I.M. (2010) BEDTools: a flexible suite of utilities for comparing genomic features. *Bioinformatics*, **26**, 841–842.
23. Zang,C., Schones,D.E., Zeng,C., Cui,K., Zhao,K. and Peng,W. (2009) A clustering approach for identification of enriched domains from histone modification ChIP-Seq data. *Bioinformatics*, **25**, 1952–1958.
24. Zhang,Y., Liu,T., Meyer,C.A., Eeckhoute,J., Johnson,D.S., Bernstein,B.E., Nusbaum,C., Myers,R.M., Brown,M., Li,W. *et al.* (2008) Model-based analysis of ChIP-Seq(MACS). *Genome Biol.*, **9**, R137.
25. Celniker,S.E., Dillon,L.A., Gerstein,M.B., Gunsalus,K.C., Henikoff,S., Karpen,G.H., Kellis,M., Lai,E.C., Lieb,J.D., MacAlpine,D.M. *et al.* (2009) Unlocking the secrets of the genome. *Nature*, **459**, 927–930.
26. Zhu,L.J., Gazin,C., Lawson,N.D., Pagès,H., Lin,S.M., Lapointe,D.S. and Green,M.R. (2010) ChIPpeakAnno: a Bioconductor package to annotate ChIP-seq and ChIP-chip data. *BMC Bioinformatics*, **11**, 237.

27. Liu,S., Yeh,C.T., Tang,H.M., Nettleton,D. and Schnable,P.S. (2012) Gene mapping via bulked segregant RNA-Seq (BSR-Seq). *PLoS ONE*, **7**, e36406.
28. Wu,T. and Nacu,S. (2010) Fast and SNP-tolerant detection of complex variants and splicing in short reads. *Bioinformatics*, **26**, 873–881.
29. Mortazavi,A., Williams,B.A., McCue,K., Schaeffer,L. and Wold,B. (2008) Mapping and quantifying mammalian transcriptomes by RNA-Seq. *Nat. Methods*, **5**, 621–628.
30. Bullard,J.H., Purdom,E., Hansen,K.D. and Dudoit,S. (2010) Evaluation of statistical methods for normalization and differential expression in mRNA-Seq experiments. *BMC Bioinformatics*, **11**, 94.
31. Lund,S.P., Nettleton,D., McCarthy,D.J. and Smyth,G.K. (2012) Detecting differential expression in RNA-sequence data using quasi-likelihood with shrunken dispersion estimates. *Stat. Appl. Genet, Mol. Biol.*, **11**, 1826.
32. Huang da,W., Sherman,B.T. and Lempicki,R.A. (2009) Systematic and integrative analysis of large gene lists using DAVID bioinformatics resources. *Nat. Protoc.*, **4**, 44–57.
33. Wickham,H. (2009) *ggplot2: Elegant Graphics for Data Analysis.* Springer Press, Heidelberg, Germany.
34. Rath,U., Wang,D., Ding,Y., Xu,Y.-Z., Qi,H., Blacketer,M.J., Girton,J., Johansen,J. and Johansen,K.M. (2004) Chromator, a novel and essential chromodomain protein interacts directly with the putative spindle matrix protein Skeletor. *J. Cell. Biochem.*, **93**, 1033–1047.
35. Cai,W., Jin,Y., Girton,J., Johansen,J. and Johansen,K.M. (2010) Preparation of polytene chromosome squashes for antibody labeling. *J. Vis. Exp.*, **36**, e1748.
36. Zhang,Y. (2007) Template-based modeling and free modeling by I-TASSER in CASP7. *Proteins*, **68**, 108–117
37. Roy,A., Kucukural,A. and Zhang,Y. (2010) I-TASSER: a unified platform for automated protein structure and function prediction. *Nat. Protoc.*, **5**, 725–738
38. Zhang,Y. (2008) Progress and challenges in protein structure prediction. *Curr. Opin. Struct. Biol.*, **18**, 342–348.
39. Yao,C., Ding,Y., Cai,W., Wang,C., Girton,J., Johansen,K.M. and Johansen,J. (2012) The chromodomain-containing NH_2-terminus of Chromator interacts with histone H1 and is required for correct targeting to chromatin. *Chromosoma*, **121**, 209–220.
40. Rath,U., Ding,Y., Deng,H., Qi,H., Bao,X., Zhang,W., Girton,J., Johansen,J. and Johansen,K.M. (2006) The chromodomain protein, Chromator, interacts with JIL-1 kinase and regulates the structure of *Drosophila* polytene chromosomes. *J. Cell Sci.*, **11**, 2332–2341.
41. Luger,K., Mader,A.W., Richmond,R.K., Sargent,D.F. and Richmond,T.J. (1997) Crystal structure of the nucleosome core particle at 2.8 Å resolution. *Nature*, **389**, 251–260.
42. Bao,X., Cai,W., Deng,H., Zhang,W., Krencik,R., Girton,J., Johansen,J. and Johansen,K.M. (2008) The COOH-terminal domain of the JIL-1 histone H3S10 kinase interacts with histone H3 and is required for correct targeting to chromatin. *J. Biol. Chem.*, **283**, 32741–32750.
43. Johansen,K.M. and Johansen,J. (2006) Regulation of chromatin structure by histone H3S10 phosphorylation. *Chromosome Res.*, **14**, 393–404.
44. Lerach,S., Zhang,W., Bao,X., Deng,H., Girton,J., Johansen,J. and Johansen,K.M. (2006) Loss-of-function alleles of the JIL-1 kinase are strong suppressors of position effect variegation of the w^{m4} allele in *Drosophila*. *Genetics*, **173**, 2403–2406.
45. Deng,H., Zhang,W., Bao,X., Martin,J.N., Girton,J., Johansen,J. and Johansen,K.M. (2005) The JIL-1 kinase regulates the structure of *Drosophila* polytene chromosomes. *Chromosoma*, **114**, 173–182.
46. Winter,S., Simboeck,E., Fischle,W., Zupkovitz,G., Dohnal,I. and Berger,S.L. (2008) 14-3-3 proteins recognize a histone code at histone H3 and are required for transcriptional activation. *EMBO J.*, **27**, 88–99.
47. Zippo,A., Serafini,R., Rocchigiani,M., Pennacchini,A., Krepelova,A. and Oliviero,S. (2009) Histone crosstalk between H3S10ph and H4K16ac generates a histone code that mediates transcription elongation. *Cell*, **138**, 1122–1136.